Environmental Science Advances

ROYAL SOCIETY OF CHEMISTRY

PAPER

View Article Online
View Journal | View Issue

Cite this: *Environ. Sci.: Adv.*, 2022, **1**, 285

Preparation, characterization, and methylene blue dye adsorption study of silk fibroin–graphene oxide nanocomposites

Lavita J. Martis, N. Parushuram and Y. Sangappa *

In the current study, an attempt was made to fabricate silk fibroin/graphene oxide (SF/GO) blend films. The obtained blend films were characterised by UV-visible spectroscopy (UV-Vis), which confirmed the blending of GO with SF. Field emission scanning electron microscopy (FE-SEM) images depicted the good distribution of GO in SF, enhancing the roughness of the film. The thermal stability of the SF/GO films was enhanced over that of native SF, as revealed by thermogravimetric analysis (TGA). Both the pristine SF and SF/GO blend films were investigated as novel methylene blue (MB) adsorbents, with good removal efficiencies of 86% and 96%, respectively. The influences of pH, contact time, concentration and adsorbent dose on the dye adsorption were systematically examined. The MB adsorption kinetics validated the pseudo-second-order model with the preferable linear fit for both the SF (R^2 = 0.995) and SF/GO blend films (R^2 = 0.993). The isotherm studies revealed that both the Freundlich and Langmuir models could accurately describe the adsorption, with the Freundlich model providing a better fit (R^2 = 0.989 (SF), R^2 = 0.997 (SF/GO)). The maximum sorption capacity for MB was estimated to be 235.84 mg g^{-1} for SF and 381.67 mg g^{-1} for the SF/GO blend films. This suggests that the as-prepared biocompatible, nontoxic SF and SF/GO blend films can serve as effective biosorbents for the treatment of dye effluents.

Received 19th December 2021
Accepted 21st April 2022

DOI: 10.1039/d1va00047k

rsc.li/esadvances

1. Introduction

In recent years, the world has been facing serious challenging threats, such as global warming, air pollution, and, more prominently, drinking water as well as ocean water pollution.[1] Water is a universal solvent and one of the most vital elements on the Earth, covering about 71% of its surface. Of the total volume of water on the Earth, 97.5% is saline, with the remaining 2.5% being fresh.[2] Unfortunately, both of these are highly polluted in several ways. Majorly, untreated wastewater, household garbage, sewage, oil leaks and agricultural wastes, when dumped into water runoff, pollute rivers, lakes, and oceans.[3] The excessive release of inorganic/organic pollutants into waterways, such as toxic metal ions and dye effluents, from the textile, leather, paper, plastic, rubber, paint, and pharmaceutical industries, also contributes significantly to pollution.[4,5] These by-products contain highly hazardous, carcinogenic, non-biodegradable, and coloured pigments that pose a great environmental problem worldwide.[6] Pollutants discharged into water runoff obstruct light penetration, which thwarts the photosynthesis of aqueous flora[7] and, as a result, endangers the lives of entire living organisms.[8,9] Even trace amounts of dye (<1 ppm) can be mutagenic and carcinogenic, rendering water unfit for human consumption.[10]

Methylene blue (MB) is a cationic dye that is commonly used to colour paper, wool, and silk,[11] and is also employed in microbiology, diagnostics, and surgery.[12] Although it is not extremely dangerous, it can have a negative impact on human health, causing an increase in heart rate, the formation of Heinz bodies, jaundice, cyanosis, and tissue necrosis.[13,14] Even brief exposure to MB can result in permanent eye damage in both humans and animals.[15] Treating effluents containing these dyes is challenging. Additionally, most conventional water-treatment techniques[16–20] have serious restrictions, including high expenses, rigorous conditions and the formation of by-products.[21,22] Therefore, it is necessary to develop a technology that is efficient, cost-effective, and nature friendly for removing dye constituents from wastewater. Recently, adsorption-based water treatment has emerged as a popular alternative to other technologies, and mainly depends on the material characteristics of the adsorbent, such as the porosity, surface-charge distribution, and surface-to-volume ratio.[23–25] Hence, there is a great interest in developing novel adsorbents with diverse configurations and advanced features. Despite being the most commonly used adsorbent for dye uptake, commercial activated charcoal is prohibitively expensive.[26] Thus, a slew of low-cost alternative bioadsorbents have been developed, including agricultural waste, silk polymorphs, coffee husk-based activated carbon,[27]

Department of Studies in Physics, Mangalore University, Mangalagangotri, Mangalore 574 199, Karnataka, India. E-mail: sangappay@gmail.com

modified rice husk,[28] sugarcane bagasse lignin,[29] cashew nut shell,[30] garlic peel,[31] orange peel,[32] calcined egg shell,[33] banana peel,[34] and natural untreated clay.[35]

In the present work, we choose silk fibroin, a natural biomass extracted by degumming *Bombyx mori* silk cocoons, which has been commonly used in the textile and biomedical fields. Their versatile properties, such as their excellent biocompatibility, biodegradability, good thermal stability, mechanical strength and minimal inflammatory response, have made SF biomaterials a popular choice for researchers seeking to employ them in technological applications.[36] The various forms of silk fibroin, such as powders, microspheres, films, and composite materials, are used for a variety of applications. Powdered silk fibroin and composite silk film, in particular, have drawn great attention as adsorbents for organic dyes because of the presence of various amino acid moieties, which endow a high adsorption capacity for MB uptake.[37,38] However, various polymorphs of fibroin with a variety of dopants have exhibited tremendous adsorption capacities over native SF.[18,39] Recently, GO, a carbon-based nanomaterial, has been mostly used in wastewater treatment as its adsorption ability towards MB is excellent.[40] The numerous oxygen-containing groups on the surface and large surface-area-to-volume ratio of GO aid in its effective interaction with dye molecules. Hence, the blending of GO with SF can result in a synergism in functionalities that provides superior performance. Although the concept of the blending of SF with GO is interesting, no reports are yet available in the literature on the systematic investigation of the development and utility of SF/GO blends as adsorbents for dye removal.

In the present study, we aim to fabricate a novel bioinspired SF/GO blend film as an efficient adsorbent for the cationic MB dye by a solvent casting technique. It is an eco-friendly, facile fabrication technique with a simple methodology that can be used to obtain a biomaterial as an adsorbent without any toxicity involved. In contrast to previous reports, an attempt has been made herein to investigate the morphology and properties of the green SF/GO blend films as well as the combined effect of SF and GO on dye adsorption systematically. Equilibrium and kinetic analyses were conducted to understand the mechanism of adsorption, and the obtained experimental data were tested with various theoretical models.

2. Experimental details

2.1 Materials

Sodium carbonate (Na_2CO_3 (>99%)) and lithium bromide (LiBr (>99%)) were purchased from Sigma Aldrich, India. All the chemicals were of analytical grade. Methylene blue ($C_{16}H_{18}N_3ClS\cdot 3H_2O$ (98%)) and graphite fine powder were purchased from Merck, India. The CB-gold silk cocoons (*Bombyx mori*) were collected from the Department of Studies in Sericulture, University of Mysore, Mysuru, India.

2.2 Preparation of SF solution

A detailed procedure for preparing the SF solution is mentioned in our previous work.[41] Briefly, fresh silk cocoons of CB-gold were chopped into small pieces (~0.2–0.3 cm) and degummed twice in 0.02 M sodium carbonate aqueous medium to separate the gum-like sericin material that covers the fibroin. The degummed SF mass was dried at room temperature after being rinsed several times with deionized water. The solution of SF was attained by immersing the dried mass in 9.3 M lithium bromide aqueous medium and heated at 60 °C for 3–4 h. To remove the lithium salts, the resultant SF–LiBr solution was dialyzed for 72 h using a dialysis cassette with a molecular weight cut-off of 3500 Da (MWCO: 3500) against deionized water. Finally, the attained clear SF solution was centrifuged at 9000 rpm to get rid of any silk aggregates and impurities that may have formed during the process. The collected 8 wt% purified SF solution was diluted to the desired wt% with double distilled water and employed for further study.

2.3 Preparation of graphene oxide

Graphene oxide (GO) was prepared from natural graphite powder using a modified Hummers' method.[42] To summarize, graphene powder (2 g) and $NaNO_3$ (1 g) were vigorously stirred in concentrated H_2SO_4 (50 mL, 98%) in a cooling bath for 2 h, yielding a black slurry. $KMnO_4$ (6 g) was then gradually added to the slurry and stirred continuously for 4 h in a cooling bath while maintaining the reaction temperature <15 °C. Following this, the above solution was stirred at 70–80 °C for another 2 h after adding 100 mL of deionized water. Further, the solution mixture was diluted with 200 mL hot water (60 °C) to maintain the pH, followed by the addition of 20 mL H_2O_2. This turned the colour of the mixture from brownish black to yellow. The acquired mixture was thoroughly washed with deionized water a number times to eliminate any residual acids present, followed by centrifugation. Finally, pure GO powder was achieved by drying the collected residue in a hot air oven at 60 °C for 24 h, and this was then used in the future analyses.

2.4 Preparation of the SF/GO blend films

To prepare the SF/GO blend films, a known amount of as-prepared GO powder (0.2 wt%) was added to the SF solution (5 wt%) in a 100 mL glass beaker. With continuous stirring for 15–20 min using a magnetic stirrer, the solution mixture was allowed to reach the desired viscosity at room temperature. The resulting mixture was then cast over polystyrene plates and allowed to stand until the films were dried completely.

3. Characterization of the samples

3.1 Optical absorption study

The optical absorption spectral study of the SF and SF/GO blend films was performed using a Shimadzu UV-1800 spectrophotometer in the 200 to 800 nm wavelength range, operated at a resolution of 1 nm at room temperature.

3.2 Surface morphological study

The surface morphology and topography of the SF and SF/GO blend films were probed with a JSM-6390 LV field emission scanning electron microscope at 15 kV. Before testing, the

samples were sputtered with gold to avoid electrical charging during the examination.

3.3 Thermal stability study

A TA instrument SDTQ 600 analyzer was used to study the thermal decomposition of the samples. All the measurements were carried out in a nitrogen atmosphere at a flow rate of 100 mL min^{-1}, with approximately 4 mg of the samples considered. At a rate of 20 °C min^{-1}, the samples were heated from lab temperature to 800 °C.

3.4 Adsorption batch experiments

The adsorption properties of the SF and SF/GO films with regards to MB removal were studied by conducting batch experiments by varying the solution pH, contact time, amount of adsorbent, and dye concentration (Table 1) and the details are given below.

To investigate the kinetics of adsorption, a predetermined amount of adsorbent (5 mg) was added to 25 mL MB solution with a fixed initial concentration (20 mg L^{-1}) contained in a series of flasks. These were monitored at room temperature for 0–24 h, with the supernatant collected every 2 h. Following that, the amount of residual MB in the collected supernatant was determined by measuring the absorbance at 664 nm with a UV-Vis absorption spectrophotometer. The amounts of sorption at time t and at equilibrium as well as the dye removal percentage were estimated with the equations provided below:[43]

$$\text{Dye removal efficiency } (\%) = \frac{(C_0 - C_e)}{C_0} \times 100 \quad (1)$$

$$q_e = \frac{(C_0 - C_e)}{M} V \quad (2)$$

where q_e accounts for the equilibrium sorption ability (mg g^{-1}) of the adsorbent, C_0 and C_e are the concentrations (mg L^{-1}) of the dye solution at the initial and equilibrium conditions, respectively, M is the amount of SF and SF/GO film (mg), and V is the volume of the testing solution (L). The obtained data were tested with different kinetic models.

For the adsorption isotherm study, 5 mg each of the SF and SF/GO films were placed in 100 mL glass flasks containing 25 mL MB solution at various initial concentrations (10–100 mg L^{-1}) and left for 24 h at lab conditions. The supernatant collected thereafter was monitored by UV-Vis absorption spectrophotometry. By fitting to the various isotherm models, the extent of dye adsorbed on the surface of the adsorbent was determined. Similarly, the influences of the adsorbent dose (6, 7, 8, and 9 mg) and pH (2–10) were also evaluated. To achieve the desired pH, 0.1 M NaOH or HCl was added to the solution.

Table 1 Conditions employed for the batch adsorption experiments

Factors	Range
pH	2–10
Time (h)	0–24
Adsorbent dose (mg)	6–9
MB concentration (mg L^{-1})	10–100

4. Results and discussion

4.1 Optical absorption study

The UV-visible absorptions of the pure SF and SF/GO blend films were recorded between 200–800 nm and the resulting spectra are shown in Fig. 1. The pure SF film displayed absorption at 275 nm, which is assigned to the π–π* transition of the tyrosine residue in the SF matrix.[37] The SF/GO blend film's spectrum exhibited peaks primarily at 237 nm and 281 nm, corresponding to graphene oxide[44] and SF, confirming the dispersion of GO in the SF matrix. *Bombyx mori*-derived SF is a fibrous protein comprising 18 different amino acids, with glycine, alanine, serine, and tyrosine residues accounting for 90% of the total. These amino acid residues in the SF backbone consist of a large number of polar groups that can effectively interact with the groups containing oxygen decorated heavily on GO.[45] The strong interactions between GO and SF result in stable, compatible SF/GO blend films. However, in the blend, a small peak at 267 nm attributed to the π-electronic conjugation and restoration of the sp^2 carbon network was observed. This implies that a small amount of GO was transformed into reduced GO after it was blended with the SF.

4.2 Surface morphological study

The surface morphology and topography of the native SF and SF/GO blend film samples were probed by SEM analysis and the corresponding images recorded are shown in Fig. 2. As seen in Fig. 2(a and b), pristine SF had a clean and smooth surface, whereas the synthesised GO had a layered wrinkle structure. The SEM images of the SF/GO blend films clearly evidence the existence of GO sheets throughout the SF matrix, implying the strong interaction between GO and SF. The dispersed GO in SF increased

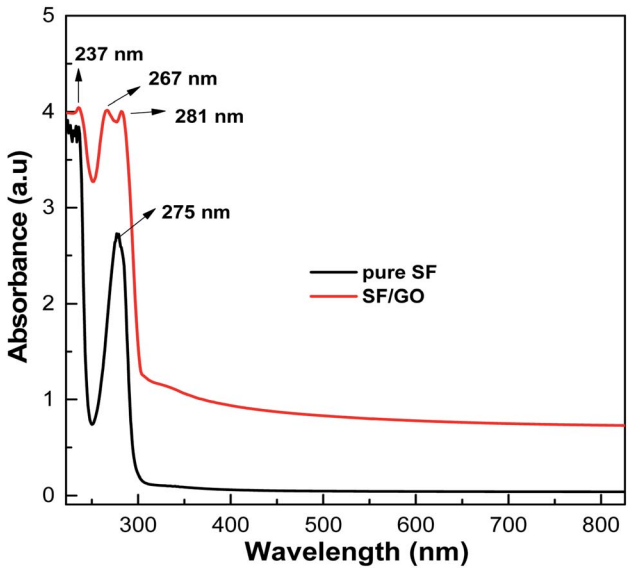

Fig. 1 UV-Vis analysis spectra of the pure SF and SF/GO blend films.

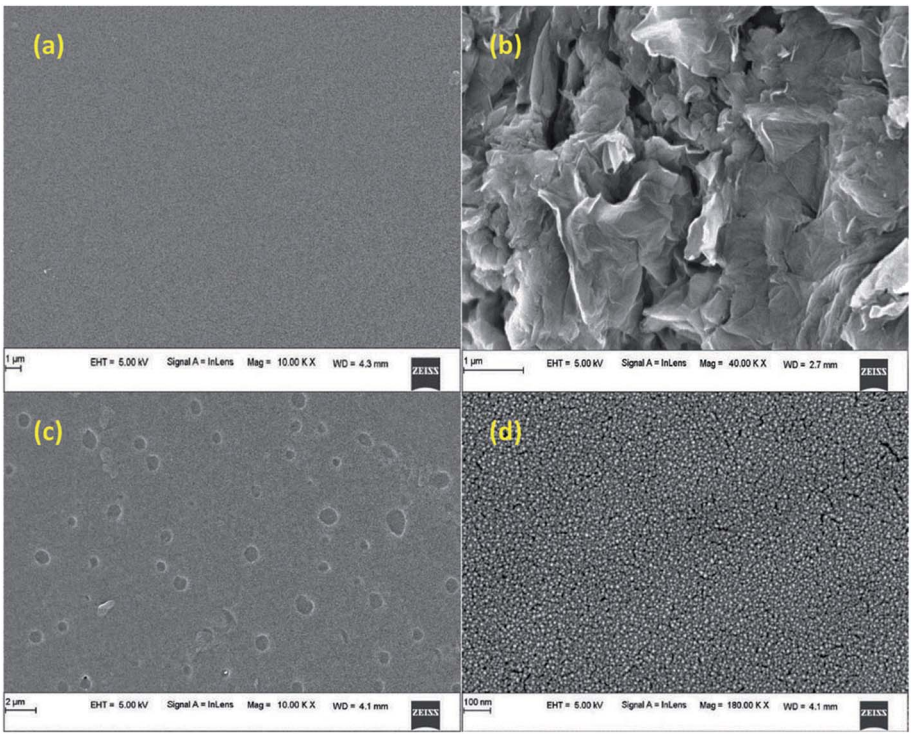

Fig. 2 SEM images of (a) pure silk fibroin, (b) pristine GO, and (c and d) the SF/GO blend film.

the surface roughness of the blend films. This in turn could greatly enhance the adsorption capacity of the blend film.[46]

4.3 Thermal stability study

The thermal stability of the native SF and SF/GO blend films was examined using thermogravimetric analysis and the corresponding TGA scans of the samples are shown in Fig. 3. According to the results, both the samples demonstrated three stages of degradation.[47] In the initial stage, the weight loss of the native SF and SF/GO films was about 17% and 12%, respectively, which occurred from room temperature to 175 °C due to the loss of water and other solvents present in the samples. The second stage of degradation of both films was recorded at temperatures ranging from 250 °C to 430 °C, where nearly 42% of the SF and 40% of the SF/GO film sample was decomposed. This can be ascribed to the interruption of the side chains as well as the cleavage of the peptide bonds in SF and SF/GO. The final stage degrades approximately 51% and 45% of the SF and SF/GO film samples, respectively. However, SF/GO exhibited enhanced thermal stability at higher temperatures when compared to pure SF, owing to the stabilisation of the blends due to GO addition.[48]

4.4 Dye adsorption study

4.4.1 Effect of pH. The solution pH, which affects the ionisation and charge on the surface of the adsorbent and adsorbate, is one of the key factors determining the sorption process. Fig. 4 presents the influence of the pH (2–10) of the aqueous media on the adsorption of MB on the SF and SF/GO films. It could be observed that the removal efficiency (at pH 2) was reduced to 7.93% and 10.06% for the SF and SF/GO films, respectively. This is mainly due to the competition between the cationic dye and the abundant H^+ ions in the acidic solution for the occupation of the binding sites on the sorbent's surface, resulting in low removal efficiency.[49] However, the percentage of dye removal increased in the pH range of 6–10, with the efficiency reaching 94% (SF) and 96% (SF/GO film). This could be attributed to the increased pH causing the association of hydroxyl ions with the adsorbent's surface, resulting in an increase in negative charge density. Furthermore, at higher pH levels, negatively charged –COO ions are easily formed as a result of the dissociation of the –COOH groups on the surface of the adsorbent. Electrostatic forces readily attract the cationic

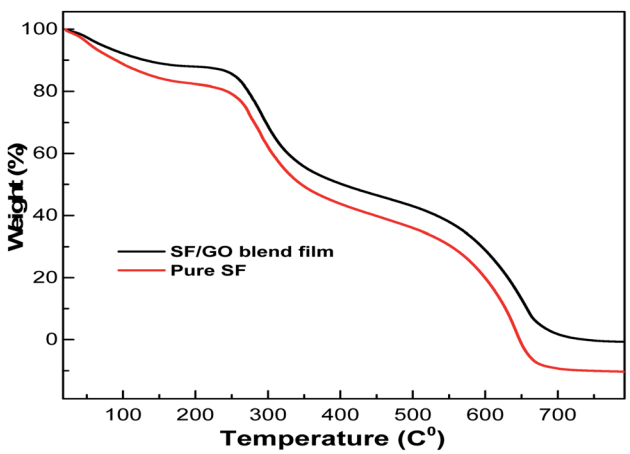

Fig. 3 TGA graphs of the pure SF and SF/GO blend films.

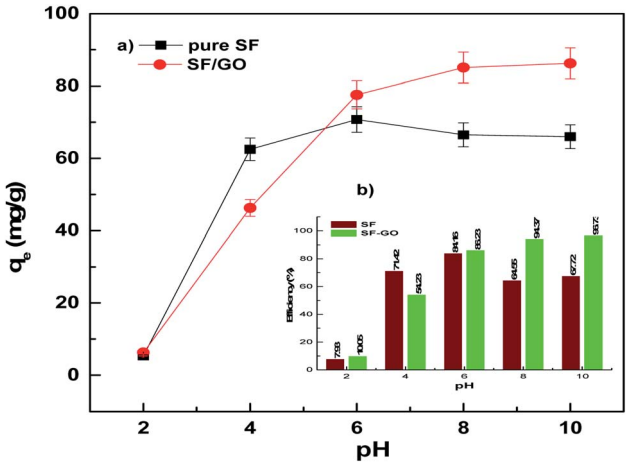

Fig. 4 (a) Adsorption capacity and (b) removal efficiency of the pure SF and SF/GO films in relation to the solution pH.

MB dye to these negatively charged functional groups of SF and SF/GO, resulting in higher removal efficiencies.[50] However, the optimal pH for this study was selected to be around 6–10.

4.4.2 Effect of contact time. The sorption ability of the SF and SF/GO films towards MB (20 mg L^{-1}) was studied over a contact time of 0 to 24 h at ambient conditions, which could be visualized by the colour change of the solutions, as shown in Fig. 5. UV-Vis spectroscopic analysis was employed to inspect the dye uptake in the presence of the SF and SF/GO films at regular intervals (step size = 2 h) and their corresponding absorption spectra are presented in Fig. 6. From the figure, it can be observed that the pure MB dye registered a characteristic absorption maximum at 664 nm with an intensity of 1.89.

After the addition of SF film to the MB solution, this peak rapidly decreased to 1.38 during the first 2 h interval (for the SF/GO film, 1.47). As the exposure time increased, a regular decolouration could be observed. After 24 h, the decolouration percentage of MB reached 86.24% for pure SF and 96.29% for the SF/GO film (Fig. 7). The equilibrium condition was reached at 22 h for both films. To confirm the attainment of adsorption equilibrium, the experiment was conducted for a 24 h contact time. From the investigation, the adsorption capacity of the SF and SF/GO films initially exhibited a relatively high adsorption capacity, but the variation in the adsorption rate became very small due to the saturation effect in the later stages. Further, due to the abundance of polar groups on SF in combination with the oxygen-containing groups on GO, the SF/GO films demonstrated enhanced adsorption efficiency over pure SF films.[46]

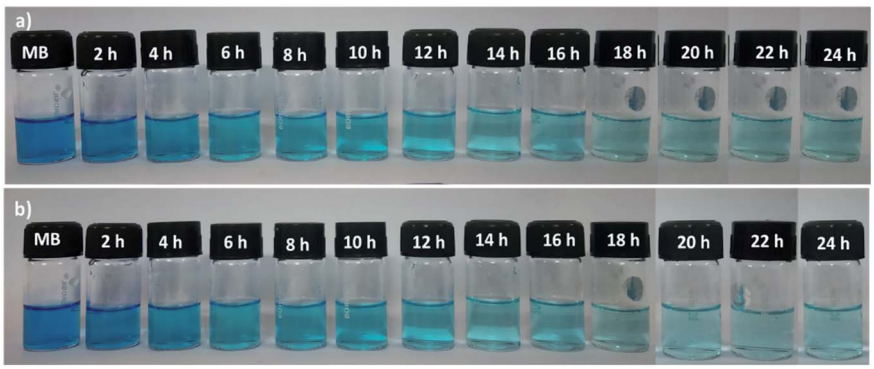

Fig. 5 Bottle image of the MB uptake on the pristine SF and SF/GO films.

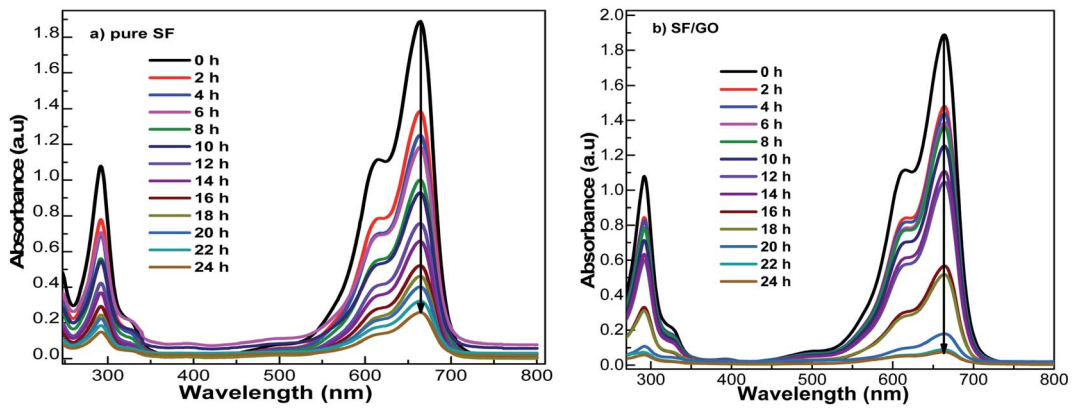

Fig. 6 UV-Vis spectral changes during MB uptake on (a) pristine SF and (b) SF/GO film at different contact times.

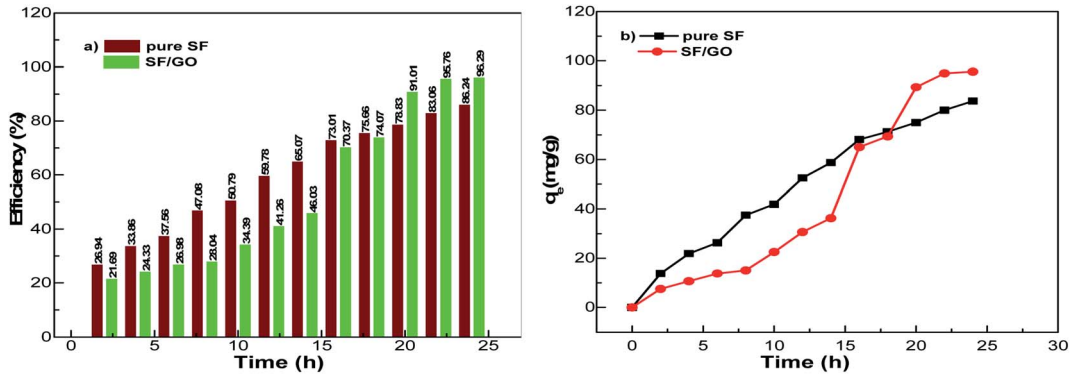

Fig. 7 (a) Efficiency and (b) adsorption capacity of the pristine SF and SF/GO films.

4.4.3 Effect of dose. In terms of practical applications, the adsorbate/adsorbent ratio is a significant parameter that must be optimized to achieve effective and economical dye removal from wastewater. The effect of the adsorbent dose on adsorption was studied by considering different amounts of sorbent (6, 7, 8, and 9 mg), and the outcomes are depicted in Fig. 8. It is noticeable from the figure that the MB uptake capacity of 6 mg each of SF and SF/GO was 35.54 and 30.23 mg g^{-1}, respectively. However, increasing the SF dose from 7 to 9 mg induced an increase in MB uptake from 42.18 to 67.75 mg g^{-1}, while the SF/GO blend film MB adsorption increased from 46.12 to 70.01 mg g^{-1}.

The results suggest that the dose-dependent MB uptake improved in the study. As expected, the availability of a larger surface area and greater number of adsorptive sites to adsorb more MB molecules with the increased loading of adsorbent resulted in enhanced dye uptake.

4.4.4 Effect of concentration. The amount of dye adsorbed on the sorbent is greatly influenced by the initial concentration of the dye considered. Fig. 9 depicts the dye removal capacity of the SF and SF/GO films with varying initial MB concentrations (10–100 mg L^{-1}). As observed, the maximum MB uptake for the SF film increased from 33.81 to 278.75 mg g^{-1}, while it increased from 44.75 to 295.52 mg g^{-1} for the SF/GO film. This implies that at higher dye concentrations, a greater mass transfer driving force facilitates a greater number of MB molecules to move towards the adsorbent surfaces and occupy the binding sites, thereby increasing the MB uptake by the adsorbents.[51]

4.4.5 Kinetic study. In the current study, the kinetic behaviour of the SF and SF/GO films towards MB was examined by employing two different kinetic models, namely the pseudo-first-order[52] and pseudo-second-order[53] models, which can be mathematically represented by eqn (3) and (4) as follows:

$$\ln(q_e - q_t) = \ln q_e - \frac{k_1}{2.303} t \quad (3)$$

$$\frac{t}{q_e} = \frac{1}{k_2 q_e^2} + \frac{1}{q_e} t \quad (4)$$

where q_e (mg g^{-1}) accounts for the amount of dye adsorbed at equilibrium while q_t (mg g^{-1}) is that at time t, and k_1 (h^{-1}) and

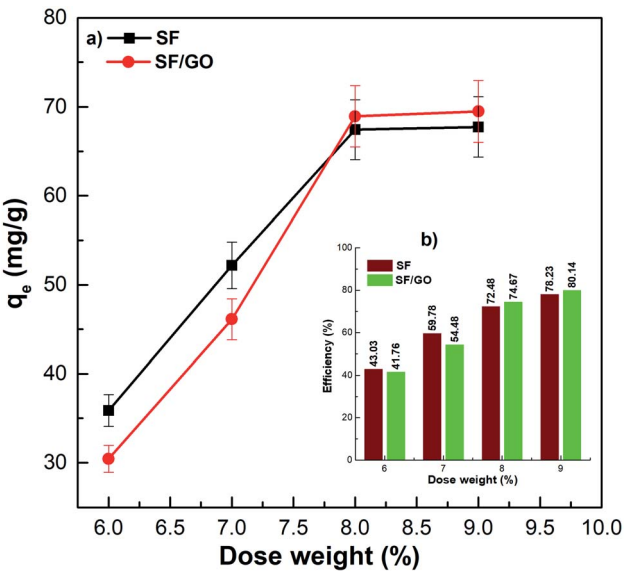

Fig. 8 (a) Adsorption capacity and (b) removal efficiency of the pure SF and SF/GO films with respect to the adsorbent dose.

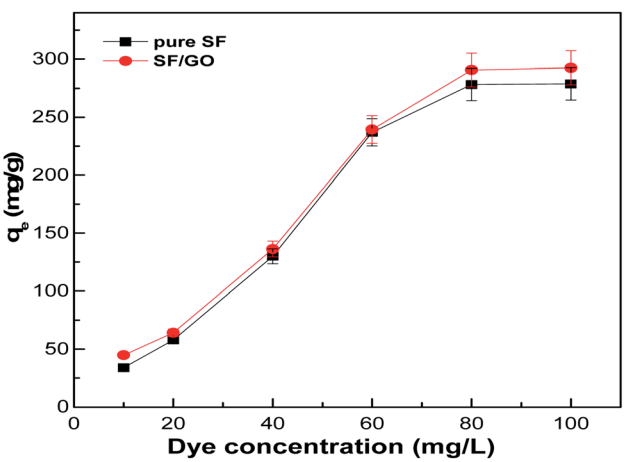

Fig. 9 Adsorption capacity with respect to the dye concentration of the pure SF and SF/GO films.

k_2 (g mg^{-1} h^{-1}) denote the rate constants corresponding to the pseudo-first and second-order kinetics. As depicted in Fig. 10, the obtained data were linearly fitted to the two kinetic models. The slopes and intercepts of the corresponding graphs were employed to determine the kinetic parameters, which are tabulated in Table 2.

From Table 2, the pseudo-first-order kinetic model predicted $q_e = 112.09$ mg g^{-1} for pure SF with a correlation of 0.916 and 142.48 mg g^{-1} for the SF/GO films with a correlation of 0.644. Whereas, for the pseudo-second-order kinetic model, the q_e and R^2 values for the SF films were 80.19 mg g^{-1} and 0.995 and for the SF/GO blend films, they were 92.34 mg g^{-1} and 0.993, respectively. However, the experimental value q_{exp} of the SF (83.75 mg g^{-1}) and SF/GO films (95.62 mg g^{-1}) were quite near to the estimated value of the pseudo-second-order kinetic model with a relatively high correlation factor. Therefore, it could be observed that the adsorption process of the SF and SF/GO films for the MB pollutant could be fitted to the pseudo-second-order kinetic model more appropriately.[54] The pseudo-second-order kinetic model is well fitted even though several probable rate limiting aspects that affect the dye adsorption kinetics were not known clearly because the adsorption mechanism of dyes on solid surfaces usually involves several steps.

Table 2 Kinetic parameters for methylene blue adsorption onto the SF and SF/GO films

Adsorbents		SF film	SF/GO film
Pseudo-first-order	k_1 (h^{-1})	0.0052	0.0043
	q_{exp} (mg g^{-1})	83.752	95.625
	q_{cal} (mg g^{-1})	112.091	142.481
	R^2	0.916	0.644
Pseudo-second-order	k_2 (g h^{-1} mg^{-1})	0.024	0.023
	q_{exp} (mg g^{-1})	83.752	95.624
	q_{cal} (mg g^{-1})	80.192	92.341
	R^2	0.995	0.993
Intraparticle diffusivity	C	3.0305	22.341
	k_1^i	18.734	5.414
	k_2^i	—	47.909
	R^2	0.981	0.996

To know the detailed aspects of the adsorption process of MB onto SF and SF/GO, the intraparticle diffusion (IPD) model propounded by Weber *et al.* was used, which can be fitted as follows[55,56]

$$q_t = k_p t^{0.5} + C \quad (5)$$

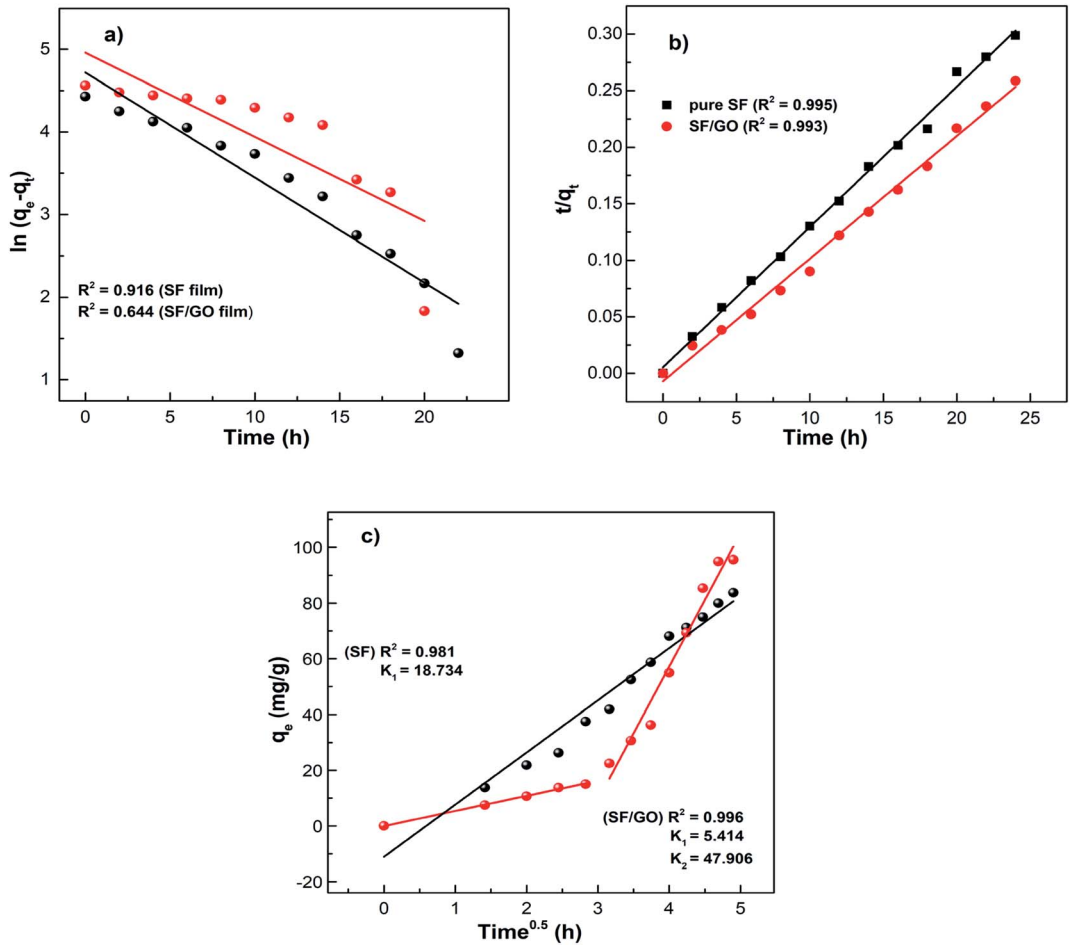

Fig. 10 MB adsorption kinetic data fitted into the (a) pseudo-first-order, (b) pseudo-second-order, and (c) intraparticle diffusion models.

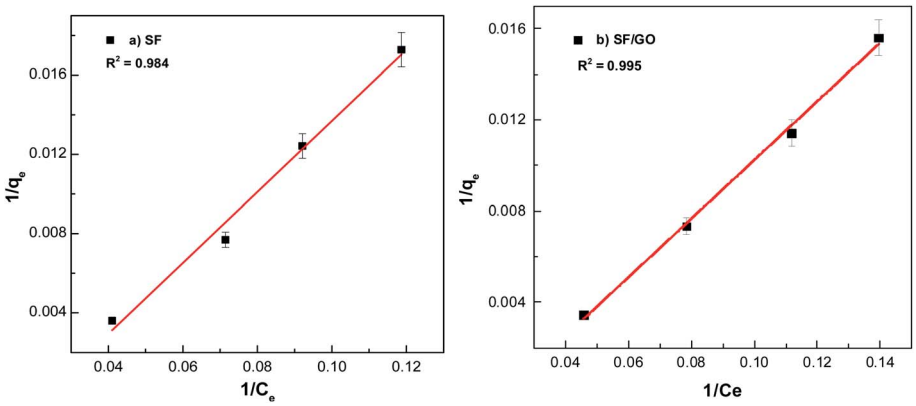

Fig. 11 Langmuir fit for the (a) pure SF and (b) SF/GO films.

where q_t represents the quantity of dye sorption at time t (mg g^{-1}), k_p denotes the rate constant of intraparticle diffusion (mg g^{-1} $h^{-1/2}$), and C represents the intercept that indicates the boundary layer thickness. If the intercept value in the linear plot of q_t *vs.* $t^{1/2}$ is zero ($C = 0$), then intraparticle diffusion becomes the rate determining step; otherwise, the various adsorption mechanisms may influence the process. The graphs of q_t *vs.* $t^{1/2}$ plotted for the SF and SF/GO films are given in Fig. 10. It can be observed that the SF film showed a single phase of adsorption, namely initial rapid uptake, which is associated with external surface adsorption in which dye molecules move on to the SF surface, whereas the SF/GO film showed a second region of adsorption, which is due to the gradual diffusion of the molecules of the dye into the pores of the sorbent material.[57]

4.4.6 Adsorption isotherms. Analysis of the adsorption isotherms is crucial in the design of any adsorbing system. In this work, the adsorption isotherms were studied by fitting the recorded equilibrium data into the Langmuir[58] and Freundlich[59] models. By comparing their correlation coefficient values, R^2, the suitability of the isotherm models to the current study was determined.

Langmuir isotherm. The Langmuir isotherm model assumes a homogeneous adsorbent surface with uniform adsorption energy facilitating monolayer coverage of the adsorbate, described by the following relation:

$$\frac{C_e}{q_e} = \frac{C_e}{q_{max}} + \frac{1}{K_L q_{max}} \quad (6)$$

where C_e indicates the concentration of the dye at the equilibrium point (mg L^{-1}), q_{max} represents the maximum adsorption capacity of the adsorbents (mg g^{-1}) corresponding to complete monolayer formation, and K_L represents the Langmuir constant, ascribed to the adsorbate's affinity towards the adsorbent (L mg^{-1}). Fig. 11 depicts the linear fits of the plotted $1/q_e$ *vs.* $1/C_e$ graphs for the pure SF and SF/GO films and the values of q_{max} and K_L determined from the slopes and intercepts of the linear plot obtained[60] are tabulated in Table 3.

Freundlich isotherm. Based on the Freundlich isotherm model, the adsorbent surface is assumed to be heterogeneous with different surface energies and follow multilayer adsorption, as expressed by the empirical formula:[61]

$$Q_e = K_F C_e^{1/n} \quad (7)$$

The above expression can be expressed in the logarithmic form as

$$\ln Q_e = \left(\frac{1}{n}\right) \ln C_e + \ln K_F \quad (8)$$

where Q_e (mg g^{-1}) denotes the quantity of dye adsorbed per unit mass of the adsorbent, C_e (mg L^{-1}) represents the equilibrium concentration of the aqueous dye solution, and K_F and n are the Freundlich isotherm constants. The value of n signifies the nature of the adsorption process, *i.e.* adsorption is linear for $n = 1$, physical for $n > 1$, and chemical for $n < 1$. The values of K_F and n can be calculated by fitting log Q_e *vs.* log C_e curves (Fig. 12). Here, the values of n for the SF (1.44) and SF/GO films (1.41) implied that the adsorption process was physical.

Table 3 Isotherm parameters for methylene blue adsorption onto the SF and SF/GO films

Adsorbents		SF film	SF/GO film
Langmuir isotherm	K_L (L mg^{-1})	0.023	0.020
	q_{max} (mg g^{-1})	235.84	381.67
	R^2	0.984	0.995
Freundlich isotherm	K_F (L g^{-1})	2.716	2.808
	n	1.44	1.41
	R^2	0.989	0.997

From Fig. 11 and 12, it can be seen that the equilibrium data fit into the Langmuir quite well, indicating a higher correlation coefficient ($R^2 = 0.984$ (SF), $R^2 = 0.995$ (SF/GO)) and high affinity constant ($K_L = 0.023$ L mg^{-1} (SF), $K_L = 0.20$ L mg^{-1} (SF/GO)). The maximum sorption capacity for MB molecules was calculated to be 235.84 mg g^{-1} for the SF and 381.67 mg g^{-1} for the SF/GO film. However, the adsorption of both the SF and SF/GO films towards MB followed the Freundlich model due to the high correlation coefficient ($R^2 = 0.989$ (SF), $R^2 = 0.997$ (SF/GO)). This might be ascribed to the surface's high roughness

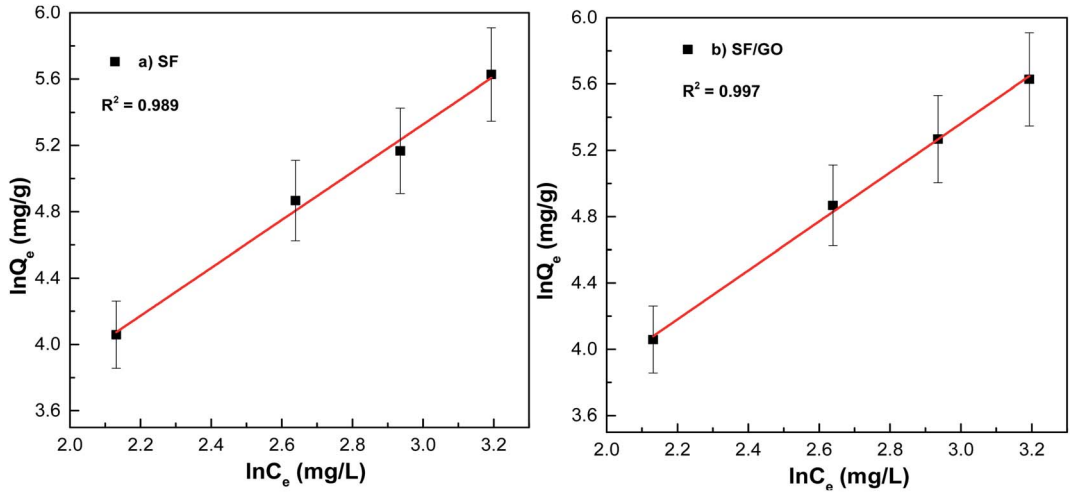

Fig. 12 Freundlich fit for the (a) pure SF and (b) SF/GO films.

and the presence of more oxidation groups, which may aid in the adsorption of MB onto the SF and SF/GO films *via* multilayer adsorption. Further, in addition to the simple electrostatic interactions, the π–π electron interactions between MB and GO can add to the greater removal efficiency of the SF/GO blend films.[62] The sorption capacity of the SF/GO blend film prepared in the present study was compared with a few previously reported low-cost silk fibroin biosorbents, as listed in Table 4. It could be observed that the SF/GO blend films exhibited significantly greater sorption capacity than most of the other fibroin biosorbents. Thus, the SF/GO blend films could serve as novel green sorbents with good adsorption capability and could be employed for the removal of dye effluents in wastewater efficiently.

4.4.7 MB removal from real water samples. To assess the practicality of the prepared SF/GO blend films, their MB removal percentage was tested for real water samples collected from tap water and river water (Phalguni), and the results are listed in Table 5. Under optimum conditions, MB of different concentrations (20, 40, and 60 mg L^{-1}) was spiked into the water samples and treated with SF/GO films. The amount of residual MB in the samples was determined using UV-Vis analysis. For comparative purposes, distilled water samples were considered as blank samples. The experimental results shown in Table 5 demonstrate that the SF/GO blend can be used as an adsorbent to efficiently remove MB from real samples.

Table 4 MB sorption capacities of a few low-cost silk fibroin biosorbents

Adsorbent	Sorption capacity (mg g^{-1})	References
Silk fibroin powder	20.58	49
Chitosan/silk fibroin/hydroxyapatite nanocomposite	476	63
Silk fibroin orange peel foam	113.8	64
Silk fibroin foam	21.8	
Silk cocoons	86.2	65
Silk microparticles	490	66
Sonicated silk microparticles	512	
Silk fibroin film	263.15	16
Silk fibroin–AuNPs NC film	313.47	
Silk fibroin film	235.12	In this study
Silk fibroin–graphene oxide film	381.62	In this study

Table 5 MB removal percentage for real samples from different sources

Sample	MB concentration (mg L^{-1})	Removal (%)
Distilled water	20	92.2
	40	87.3
	60	80.6
Tap water	20	90.5
	40	85.2
	60	78.5
River water	20	91.8
	40	86.1
	60	80.7

5. Conclusion

In the present work, a silk fibroin/graphene oxide (SF/GO) blend film was fabricated successfully and used as an effective adsorbent for the removal of MB. UV-Vis analysis confirmed the blending of GO with SF. The morphological studies of the films by FE-SEM showed the good distribution of GO in SF. The thermal stability of the SF/GO film was enhanced over that of pure SF. The dye adsorption study revealed that the adsorption capacity was pH- and dose-dependent, with the MB removal capacity increasing with pH (>6) and the adsorbent dose for both the SF and SF/GO blend films. The removal efficiency was observed to be 86% for SF and 96% for the SF/GO blend film. The kinetics of the adsorption of MB was found to follow the

pseudo-second-order model. The dye adsorption equilibrium data were tested in the Langmuir and Freundlich models, giving a best fit with the Freundlich model, showing that the adsorption was multilayer. The high removal efficiency, along with its eco-friendly nature and ease of preparation, makes SF/GO a preferable choice as an absorbent for wastewater treatment compared to other low-cost adsorbents.

Author contributions

LJM: data collection, writing and original draft preparation, plotting graphs, visualization. PN: experimental assistance, editing. SY: conceptualization, methodology and supervision.

Conflicts of interest

Authors declare no conflicts of interest.

Acknowledgements

One of the authors acknowledges the financial support received from the Directorate of Minorities, Govt. of Karnataka, India.

References

1 R. K. Mishra and S. C. Dubey, Fresh water availability and its global challenge, *Int. J. Eng. Sci. Invention Res. Dev.*, 2015, **2**, 351–407.
2 K. N. Kikkas and S. V. Kulik, Modelling the effect of human activity on fresh water extraction from the earth's reserves, *IOP Conf. Ser.: Earth Environ. Sci.*, 2018, **180**, 012017.
3 D. Bhatia, N. R. Sharma, J. Singh and R. S. Kanwar, Biological methods for textile dye removal from wastewater: a review, *Crit. Rev. Environ. Sci. Technol.*, 2017, **47**, 1836–1876.
4 N. Kannan and M. M. Sundaram, Kinetics and mechanism of removal of methylene blue by adsorption on various carbons - a comparative study, *Dyes Pigm.*, 2001, **51**(1), 25–40.
5 M. S. Tehrani and R. Zare-Dorabei, Highly efficient simultaneous ultrasonic-assisted adsorption of methylene blue and rhodamine B onto metal organic framework MIL-68(Al): Central composite design optimization, *RSC Adv.*, 2016, **6**, 27416–27425.
6 H. P. de Carvalho, J. Huang, M. Zhao, G. Liu, L. Dong and X. Liu, Improvement of methylene blue removal by electrocoagulation/banana peel adsorption coupling in a batch system, *Alexandria Eng. J.*, 2015, **54**(3), 777–786.
7 Y. S. Al-Degs, M. I. El-Barghouthi, A. H. El-Sheikh and G. M. Walker, Effect of solution pH, ionic strength, and temperature on adsorption behaviour of reactive dyes on activated carbon, *Dyes Pigm.*, 2008, **77**, 16–23.
8 K. Singh and S. Arora, Removal of synthetic textile dyes from wastewaters: a critical review on present treatment technologies, *Crit. Rev. Environ. Sci. Technol.*, 2011, **41**(9), 807–878.
9 A. Kiani, P. Haratipour, M. Ahmadi, R. Zare-Dorabei and A. Mahmoodi, Efficient removal of some anionic dyes from aqueous solution using a polymer-coated magnetic nano-adsorbent, *J. Water Supply: Res. Technol.–AQUA*, 2017, **66**(4), 239–248.
10 R. O. A. De Lima, A. P. Bazo, D. M. F. Salvadori, C. M. Rech, D. P. Oliveira and G. A. Umbuzeiro, Matagenic and carcinogenic potential of a textile azo dye processing plant effluent that impacts a drinking water source, *Mutat. Res., Genet. Toxicol. Environ. Mutagen.*, 2007, **626**, 53–60.
11 M. M. Hamed, I. M. Ahmed and S. S. Metwally, Adsorptive removal of methylene blue as organic pollutant by marble dust as eco-friendly sorbent, *J. Ind. Eng. Chem.*, 2014, **20**(4), 2370–2377.
12 A. Milani, A. M. Ciammella, C. Degen, M. Siciliano and L. Rossi, Ascites dynamics in cirrhosis: Proposal and validation of a methylene blue dilution test, *J. Hepatol.*, 1992, **16**(3), 369–375.
13 D. K. Mahmoud, M. A. M. Salleh, W. A. W. A. Karim, A. Idris and Z. Z. Abidin, Batch adsorption of basic dye using acid treated kenaf fibre char: equilibrium, kinetic and thermodynamic studies, *Chem. Eng. J.*, 2012, **181**, 449–457.
14 M. Rafatullah, O. Sulaiman, R. Hashim and A. Ahmad, Adsorption of methylene blue on low-cost adsorbents: a review, *J. Hazard. Mater.*, 2010, **177**(1–3), 70–80.
15 V. M. Vučurović, R. N. Razmovski and M. N. Tekić, Methylene blue (cationic dye) adsorption onto sugar beet pulp: equilibrium isotherm and kinetic studies, *J. Taiwan Inst. Chem. Eng.*, 2012, **43**(1), 108–111.
16 S. Altenor, B. Carene, E. Emmanuel, J. Lambert, J. J. Ehrhardt and S. Gaspard, Adsorption studies of methylene blue and phenol onto vetiver roots activated carbon prepared by chemical activation, *J. Hazard. Mater.*, 2009, **165**(1–3), 1029–1039.
17 E. B. Butler, Y. T. Hung and O. Mulamba, The effects of chemical coagulants on the decolorization of dyes by electrocoagulation using response surface methodology, *Appl. Water Sci.*, 2017, **7**(5), 2357–2371.
18 N. Parushuram, R. Ranjana, K. S. Harisha, M. Shilpa, B. Narayana, R. Neelakandan and Y. Sangappa, Silk fibroin and silk fibroin-gold nanoparticles nanocomposite films: sustainable adsorbents for methylene blue dye, *J. Dispersion Sci. Technol.*, 2020, 1–16, DOI: **10.1080/01932691.2020.1848578**.
19 M. Hu and B. Mi, Enabling graphene oxide nanosheets as water separation membranes, *Environ. Sci. Technol.*, 2013, **47**(8), 3715–3723.
20 J. Labanda, J. Sabaté and J. Llorens, Modeling of the dynamic adsorption of an anionic dye through ion-exchange membrane adsorber, *J. Membr. Sci.*, 2009, **340**(1–2), 234–240.
21 M. Yazdanbakhsh, H. Tavakkoli and S. M. Hosseini, Characterization and evaluation catalytic efficiency of $La_{0.5}Ca_{0.5}NiO_3$ nanopowders in removal of reactive blue 5 from aqueous solution, *Desalination*, 2011, **281**, 388–395.
22 T. Tabari, H. Tavakkoli, P. Zargaran and D. Beiknejad, Fabrication of perovskite-type oxide $BaPbO_3$ nanoparticles and their efficiency in photodegradation of methylene blue, *S. Afr. J. Chem.*, 2012, **65**(1), 239–244.
23 S. Nourozi and R. Zare-Dorabei, Highly efficient ultrasonic-assisted removal of methylene blue from aqueous media

by magnetic mesoporous silica: experimental design methodology, kinetic and equilibrium studies, *Desalin. Water Treat.*, 2017, **85**, 184–196.

24 F. Ramezani and R. Zare-Dorabei, Simultaneous ultrasonic-assisted removal of malachite green and methylene blue from aqueous solution by Zr-SBA-15, *Polyhedron*, 2019, **166**, 153–161.

25 M. S. Tehrani and R. Zare-Dorabei, Competitive removal of hazardous dyes from aqueous solution by MIL-68(Al); derivative spectrophotometric method and response surface methodology approach, *Spectrochim. Acta, Part A*, 2016, **160**, 8–18.

26 A. O. Alade, O. S. Amuda, T. J. Afolabi and A. A. Okoya, Adsorption of Naphthalene onto Activated Carbons Derived from Milk Bush Kernel Shell and Flamboyant Pod, *J. Environ. Chem. Ecotoxicol.*, 2012, **4**, 124–132.

27 M. A. Ahmad and N. K. Rahman, Equilibrium, kinetics and thermodynamic of Remazol Brilliant Orange 3R dye adsorption on coffee husk-based activated carbon, *Chem. Eng. J.*, 2011, **170**(1), 154–161.

28 M. A. Rahman, S. R. Amin and A. S. Alam, Removal of methylene blue from waste water using activated carbon prepared from rice husk, *Dhaka Univ. J. Sci.*, 2012, **60**(2), 185–189.

29 L. G. Da Silva, R. Ruggiero, P. M. Gontijo, R. B. Pinto, B. Royer, E. C. Lima, T. H. M. Fernandes and T. Calvete, Adsorption of Brilliant Red 2BE Dye from Water Solutions by Chemically Modified Sugarcane Bagasse Lignin, *Chem. Eng. J.*, 2011, **168**, 620–628.

30 P. S. Kumar, S. Ramalingam, C. Senthamarai, M. Niranjanaa, P. Vijayalakshmi and S. Sivanesan, Adsorption of dye from aqueous solution by cashew nut shell: studies on equilibrium isotherm, kinetics and thermodynamics of interactions, *Desalination*, 2010, **261**(1–2), 52–60.

31 B. H. Hameed and A. A. Ahmad, Batch adsorption of methylene blue from aqueous solution by garlic peel, an agricultural waste biomass, *J. Hazard. Mater.*, 2009, **164**(2–3), 870–875.

32 C. Namasivayam, N. Muniasamy, K. Gayatri, M. Rani and K. Ranganathan, Removal of dyes from aqueous solutions by cellulosic waste orange peel, *Bioresour. Technol.*, 1996, **57**(1), 37–43.

33 R. Slimani, I. El Ouahabi, F. Abidi, M. El Haddad, A. Regti, M. R. Laamari, S. El Antri and S. Lazar, Calcined eggshells as a new biosorbent to remove basic dye from aqueous solutions: thermodynamics, kinetics, isotherms and error analysis, *J. Taiwan Inst. Chem. Eng.*, 2014, **45**(4), 1578–1587.

34 C. Namasivayam and N. Kanchana, Waste banana pith as adsorbent for color removal from wastewaters, *Chemosphere*, 1992, **25**(11), 1691–1705.

35 E. Errais, J. Duplay, F. Darragi, I. M'Rabet, A. Aubert, F. Huber and G. Morvan, Efficient anionic dye adsorption on natural untreated clay: kinetic study and thermodynamic parameters, *Desalination*, 2011, **275**, 74–81.

36 Y. Sangappa, S. Latha, S. Asha, P. Sindhu, N. Parushuram, M. Shilpa, K. Byrappa and B. Narayana, Synthesis of anisotropic silver nanoparticles using silk fibroin: characterization and antimicrobial properties, *Mater. Res. Innovations*, 2019, **23**(2), 79–85.

37 E. Wenk, H. P. Merkle and L. Meinel, Silk fibroin as a vehicle for drug delivery applications, *J. Controlled Release*, 2011, **150**(2), 128–141.

38 K. S. Harisha, N. Parushuram, S. Asha, S. B. Suma, B. Narayana and Y. Sangappa, Eco-synthesis of gold nanoparticles by Sericin derived from Bombyx mori silk and catalytic study on degradation of methylene blue, *Part. Sci. Technol.*, 2021, **39**(2), 131–140.

39 S. Wang, H. Ning, N. Hu, K. Huang, S. Weng, X. Wu, L. Wu, J. Liu and Alamusi, Preparation and characterization of graphene oxide/silk fibroin hybrid aerogel for due and heavy metal adsorption, *Composites, Part B*, 2019, **163**, 716–722.

40 Y. Li, Q. Du, X. Peng, J. Wang, J. Sun, Y. Wang, S. Wu, Z. Wang, Y. Xia and L. Xia, Comparative study of methylene blue dye adsorption onto activated carbon, graphene oxide, and carbon nanotubes, *Chem. Eng. Res. Des.*, 2013, **91**, 361–368.

41 P. Nilogal, G. B. Uppine, R. Rayaraddi, H. K. Sanjeevappa, L. J. Martis, B. Narayana and Y. Sangappa, Conductive in situ reduced graphene oxide–silk fibroin bionanocomposites, *ACS Omega*, 2021, **6**(20), 12995–13007.

42 J. Chen, Y. Li, L. Huang, C. Li and G. Shi, High-yield preparation of graphene oxide from small graphite flakes via an improved Hummers method with a simple purification process, *Carbon*, 2015, **81**, 826–834.

43 A. Arabpour, S. Dan and H. Hashemipour, Preparation and optimization of novel graphene oxide and adsorption isotherm study of methylene blue, *Arabian J. Chem.*, 2021, **14**, 103003.

44 S. B. Maddinedi, B. K. Mandal, R. Vankayala, P. Kalluru and S. R. Pamanji, Bioinspired reduced graphene oxide nanosheets using *Terminalia chebula* seeds extract, *Spectrochim. Acta, Part A*, 2015, **145**, 117–124.

45 K. Li, P. Li and Y. Fan, The assembly of silk fibroin and graphene-based nanomaterials with enhanced mechanical/conductive properties and their biomedical applications, *J. Mater. Chem. B*, 2019, **7**, 6890.

46 L. Wang, C. Lu, B. Zhang, B. Zhao, F. Wu and S. Guan, Fabrication and characterization of flexible silk fibroin films reinforced with graphene oxide for biomedical applications, *RSC Adv.*, 2014, **4**, 40312.

47 R. Ranjana, N. Parushuram, K. S. Harisha, S. Asha, B. Narayana, M. Mahendra and Y. Sangappa, Fabrication and characterization of conductive silk fibroin-gold nanocomposite films, *J. Mater. Sci.: Mater. Electron.*, 2020, **31**, 249–264.

48 M. El Achaby, F. Z. Arrakhiz, S. Vaudreuil, E. M. Essassi and A. Qaiss, Piezoelectric β-polymorph formation and properties enhancement in graphene oxide–PVDF nanocomposite films, *Appl. Surf. Sci.*, 2012, **258**(19), 7668–7677.

49 S. Xiao, Z. Wang, H. Ma, H. Yang and W. Xu, Effective removal of dyes from aqueous solution using ultrafine silk fibroin powder, *Adv. Powder Technol.*, 2014, **25**, 574–581.

50 M. Saxena, N. Sharm and R. Saxena, Highly efficient and rapid removal of a toxic dye: adsorption kinetics, isotherm, and mechanism studies on functionalized multiwalled carbon nanotubes, *Surf. Interfaces*, 2020, **21**, 100639.
51 N. P. Raval, P. U. Shah and N. K. Shah, Nanoparticles loaded biopolymer as effective adsorbent for adsorptive removal of malachite green aqueous solution, *Water Conserv. Sci. Eng.*, 2016, **1**, 69–81.
52 Y. R. Zhang, S. Q. Wang, S. L. Shen and B. X. Zhao, A novel water treatment magnetic nanomaterial for removal of anionic and cationic dyes under severe condition, *Chem. Eng. J.*, 2013, **233**, 258–264.
53 Y. R. Zhang, S. L. Shen, S. Q. Wang, J. Huang, P. Su, Q. R. Wang and B. X. Zhao, A dual function magnetic nanomaterial modified with lysine for removal of organic dyes from water solution, *Chem. Eng. J.*, 2014, **239**, 250–256.
54 P. R. Chang, P. Zheng, B. Liu, D. P. Anderson, J. Yu and X. Ma, Characterization of magnetic soluble starch-functionalized carbon nanotubes and its application for the adsorption of the dyes, *J. Hazard. Mater.*, 2011, **186**(2–3), 2144–2150.
55 P. Ajitha, K. Vijayalakshmi, M. Saranya, T. Gomathi, K. Rani, P. N. Sudha and A. Sukumaran, Removal of toxic heavy metal lead (II) using chitosan oligosaccharide-graft-maleic anhydride/polyvinyl alcohol/silk fibroin composite, *Int. J. Biol. Macromol.*, 2017, **104**, 1469–1482.
56 M. Dogan, M. Alkan, A. Türkyilmaz and Y. Ozdemir, Kinetics and mechanism of removal of methylene blue by adsorption onto perlite, *J. Hazard. Mater.*, 2004, **109**(1–3), 141–148.
57 Z. Zhang, X. Zhao, X. Jv, H. Lu and L. Zhu, A simplified method for synthesis of l-tyrosine modified magnetite nanoparticles and its application for the removal of organic dyes, *J. Chem. Eng. Data*, 2017, **62**(12), 4279–4287.
58 B. H. Hameed, A. M. Din and A. L. Ahmad, Adsorption of methylene blue onto bamboo-based activated carbon: kinetics and equilibrium studies, *J. Hazard. Mater.*, 2007, **141**(3), 819–825.
59 S. Rastogi and B. Kandasubramanian, Progressive trends in heavy metal ions and dyes adsorption using silk fibroin composites, *Environ. Sci. Pollut. Res.*, 2020, **27**(1), 210–237.
60 A. K. Kodoth and V. Badalamoole, Silver nanoparticle-embedded pectin-based hydrogel for adsorptive removal of dyes and metal ions, *Polym. Bull.*, 2020, **77**(2), 541–564.
61 P. G. Bhavyashree and T. S. Xavier, Adsorption studies of methylene blue, coomassie brilliant blue, and congo red dyes onto Cu/O nanocomposites synthesized via *Vitex negundo* linn leaf extract, *Curr. Opin. Green Sustainable Chem.*, 2021, **4**, 100161.
62 T. Wu, X. Cai, S. Tan, H. Li, J. Liu and W. Yang, Adsorption characteristics of acrylonitrile, p-toulenesulfonic acid, 1-naphthalenesulfonic acid and methyl blue on graphene in aqueous solutions, *Chem. Eng. J.*, 2011, **173**, 144–149.
63 A. Salama, K. R. Shoueir and H. A. Aljohani, Preparation of sustainable nanocomposite as new adsorbent for dyes removal, *Fibers Polym.*, 2017, **18**, 1825–1830.
64 L. Campagnolo, D. Morselli, D. Magri, A. Scarpellini, C. Demirci, M. Colombo, A. Athanassia and D. Fragouli, Silk fibroin/orange peel foam: an efficient biocomposite for water remediation, *Adv. Sustainable Syst.*, 2018, **3**, 1800097.
65 N. S. Tabrizi and M. Yavari, Adsorption of methylene blue from aqueous solutions by silk cocoon, *Int. J. Eng.*, 2016, **29**, 1191–1197.
66 N. Parushuram, R. Ranjana, B. Narayana, M. Mahendra and Y. Sangappa, Facile fabrication of silk fibroin microparticles: their characterization and potential adsorption study, *J. Dispersion Sci. Technol.*, 2020, **42**, 1513–1531.